



Faculty of Liberal Arts & Sciences

2024

A Tale of Three Dwarfs: Cluster-based Star Formation Histories of Blue Compact Dwarf Galaxies

Chandar, Rupali, Caputo, Miranda, Mok, Angus, Linden, Sean, Whitmore, Bradley C., Goudfrooij, Paul, Cook, David O., Calzetti, Daniela, Elmegreen, Debra M., Lee, Janice C., Úbeda, Leonardo and White, Richard

Suggested citation:

Chandar, Rupali, Caputo, Miranda, Mok, Angus, Linden, Sean, Whitmore, Bradley C., Goudfrooij, Paul, Cook, David O., Calzetti, Daniela, Elmegreen, Debra M., Lee, Janice C., Úbeda, Leonardo and White, Richard (2024) A Tale of Three Dwarfs: Cluster-based Star Formation Histories of Blue Compact Dwarf Galaxies. *The Astrophysical Journal*, 965 (1). p. 95. ISSN 0004-637X Available at <https://openresearch.ocadu.ca/id/eprint/4521/>

Open Research is a publicly accessible, curated repository for the preservation and dissemination of scholarly and creative output of the OCAD University community. Material in Open Research is open access and made available via the consent of the author and/or rights holder on a non-exclusive basis.

The OCAD University Library is committed to accessibility as outlined in the [Ontario Human Rights Code](#) and the [Accessibility for Ontarians with Disabilities Act \(AODA\)](#) and is working to improve accessibility of the Open Research Repository collection. If you require an accessible version of a repository item contact us at repository@ocadu.ca.



A Tale of Three Dwarfs: Cluster-based Star Formation Histories of Blue Compact Dwarf Galaxies

Rupali Chandar¹, Miranda Caputo¹, Angus Mok², Sean Linden³, Bradley C. Whitmore⁴, Paul Goudfrooij⁴, David O. Cook⁵, Daniela Calzetti³, Debra M. Elmegreen⁶, Janice C. Lee⁷, Leonardo Úbeda⁴, and Richard White⁴

¹Ritter Astrophysical Research Center, University of Toledo, Toledo, OH 43606, USA; rupali.chandar@utoledo.edu

²OCAD University, Toronto, Ontario, M5T 1W1, Canada

³Dept. of Astronomy, University of Massachusetts at Amherst, Amherst, MA 01003, USA

⁴Space Telescope Science Institute, 3700 San Martin Drive, Baltimore, MD, 21218, USA

⁵Caltech/IPAC, 1200 E. California Boulevard, Pasadena, CA 91125, USA

⁶Department of Physics & Astronomy, Vassar College, Poughkeepsie, NY 12604, USA

⁷Gemini Observatory/NSFs NOIRLab, 950 N. Cherry Avenue, Tucson, AZ, 85719, USA

Received 2023 July 13; revised 2024 January 27; accepted 2024 February 12; published 2024 April 10

Abstract

We present a new study of the cluster populations in the blue compact dwarf galaxies (BCD) ESO185-IG13, ESO338-IG04, and Haro11, based on new and archival high-resolution images taken by the Hubble Space Telescope, and the first to probe the populations older than ≈ 100 Myr. BCDs are believed to experience intense bursts of star formation (including at the present day) after long periods of quiescence, but little is known about the timing, frequency, duration, and strength of these bursts or about their star formation histories in general. We find that the cluster population in each of the three galaxies studied here has its own unique distribution of colors and hence a unique cluster and star formation history. From an assumed correlation between the normalization of the cluster mass function and the star formation rate of the host galaxy, we construct cluster-based star formation histories over the past $\approx \text{few} \times \text{Gyr}$ and find that only Haro11 is currently experiencing a burst (\approx factor of 10 increase in the rate of star formation for the last ≈ 20 Myr), whereas ESO185 experienced enhanced star formation (by a factor ≈ 4) between 10 and 40 Myr ago, and ESO338 has had a fairly constant SFH over the past few Gyr. These findings indicate that not all BCDs are experiencing a burst of star formation at the present day, and that some have been forming stars and clusters at a fairly steady rate (within a factor of $\approx 2-3$) over the past few Gyr. This scenario is similar to the histories of dwarf irregular and dwarf starburst galaxies, which have star formation rates that are 10–1000 times lower than those in BCDs.

Unified Astronomy Thesaurus concepts: [Galaxy evolution \(594\)](#)

1. Introduction

Blue compact dwarfs (BCDs) are small, clumpy galaxies that are experiencing intense star formation (e.g., Sargent 1970; Kunth et al. 1988; Thuan & Izotov 2005; Bekki et al. 2010). Some BCDs, like Haro11, have distinct star-forming knots with physical sizes of a few hundred pc that are dominated by different-age stars and clusters (Sirressi et al. 2022). Somewhat unusually for such intensely star-forming galaxies, BCDs do not contain much dust or many metals (Mas-Hesse & Kunth 1999), and they are about 1/10 the size (1/100 the area) of typical spiral galaxies like the Milky Way. These small galaxies are of particular interest in galaxy evolution because they share many of the properties observed in high-redshift galaxies (e.g., Hoopes et al. 2007; Cairós et al. 2010; Chen et al. 2023; Hainline et al. 2024).

BCDs are believed to have experienced long periods with little activity punctuated by short-lived, violent bursts of star formation (Fanelli et al. 1988; Zhao et al. 2011). Analysis of their integrated light indicates that many of these galaxies are experiencing an intense burst of star formation right now (e.g., Papaderos et al. 2008). This view is supported by previous analyses of the cluster populations in a number of blue compact

dwarf (BCD) galaxies, where it was suggested that the rate of cluster and hence star formation peaked in the last 10 Myr in ESO 185 (Adamo et al. 2011b), ESO338 (Östlin et al. 2003; Adamo et al. 2011a), and Haro 11 (Adamo et al. 2010), among others (e.g., Silich et al. 2002; Contreras Ramos et al. 2011; Olsen et al. 2021). Two timescales are likely relevant for bursts: $\approx 5-10$ Myr (comparable to the lifetime of massive stars) and $\approx \text{few tens of Myr}$ (the crossing time of star-forming knots). A burst of star formation produces strong feedback in the form of stellar winds, supernova explosions, etc., that might disrupt the gas that fuels star formation and extinguish the starburst on the timescale of a few to ten Myr, according to observations (e.g., Mas-Hesse & Kunth 1999; Schaerer et al. 1999; Thornley et al. 2000; Tremonti et al. 2001; Harris et al. 2004) and theory (e.g., Tosi et al. 1989; Ferguson & Babul 1998; Stinson et al. 2007). A longer timescale of roughly a few tens of Myr may also be possible, as this is the crossing time of star-forming knots, which have sizes $\approx \text{few} \times 100$ pc.

We know now that short, intense bursts of star formation are rare in dwarf irregular and starburst galaxies, which are forming stars at rates 10–10,000 times lower than BCDs. These galaxies experience star formation that is continuous within a factor of 2–3, and with no rapid “self-quenching” (McQuinn et al. 2010a; Cignoni et al. 2019). Because many normal galaxies experience variations in their rate of star formation at this level, in this work we consider a “burst” to be a much more



Original content from this work may be used under the terms of the [Creative Commons Attribution 4.0 licence](#). Any further distribution of this work must maintain attribution to the author(s) and the title of the work, journal citation and DOI.

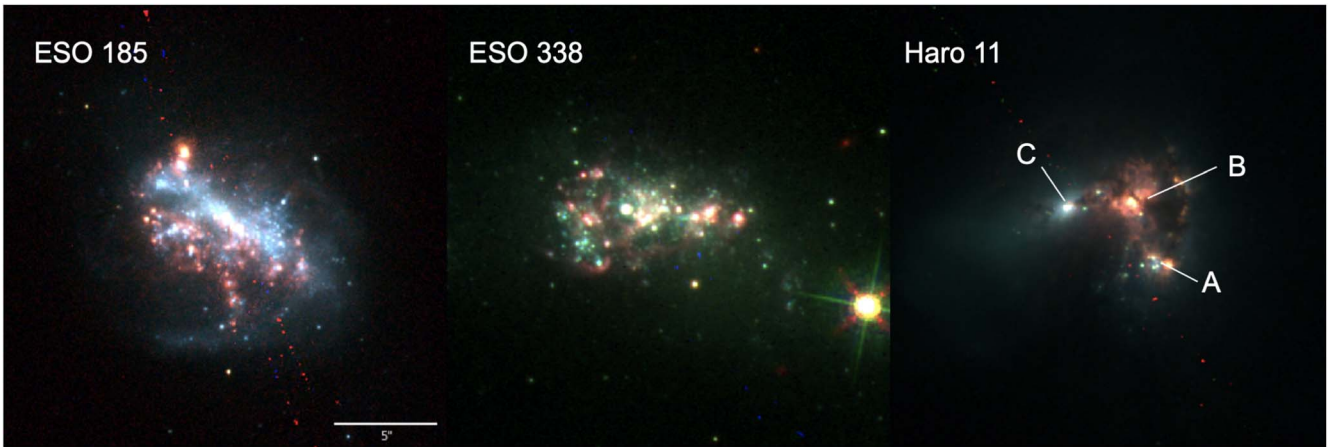


Figure 1. Three-color HST images of the blue compact dwarf galaxies in this study. For ESO185 and Haro11, the red channel shows $H\alpha$ emission, and for ESO338, this channel shows $Pa\beta$ because no $H\alpha$ imaging exists. Knots of star formation appear red and highlight the locations where star formation is currently taking place. The scale bar in the left panel is $5''$ long, and represents 1.8 kpc, 0.9 kpc, and 2.0 kpc in ESO185, ESO338, and Haro 11, respectively.

Table 1
Blue Compact Dwarf Galaxy Sample

Galaxy Name	Distance (Mpc)	Foreground $E(B - V)$ (mag)	SFR ^a ($M_{\odot} \text{ yr}^{-1}$)	Area (kpc^2)	Σ_{SFR} ($M_{\odot} \text{ yr}^{-1} \text{ kpc}^{-2}$)
ESO 185	76	0.048	4.6	12.3	0.38
ESO 338	38	0.076	2.3	2.0	1.15
Haro11	82	0.010	17.4	10.2	1.70

Note.

^a The original star formation rates published in Adamo et al. (2011a) have been divided by 1.38 to convert from an assumed Salpeter to the more modern Chabrier stellar initial mass function.

significant increase, by a factor of ≈ 10 or more, in its star formation rate. Compared to dwarf irregular and dwarf starburst galaxies, BCDs have especially compact stellar and H I distributions (Papaderos et al. 1996; van Zee et al. 1998; Janowiecki & Salzer 2014; Lelli et al. 2014). It is possible that this compact distribution enables more efficient bursts that reach significantly higher rates of star formation.

A number of open questions about the star formation histories of BCDs remain. Are all BCDs currently experiencing a burst of star and cluster formation? What is the typical timing, duration, strength, and frequency of star-forming bursts in BCDs? How do their SFHs compare with their less intensely star-forming cousins, dwarf starburst and irregular galaxies? In this work, we address these questions by determining the first star formation histories of ESO185-IG13 and ESO338-IG04, hereafter referred to as ESO185 and ESO338, as well as Haro11, three BCD galaxies observed with the Hubble Space Telescope (HST) as part of the ‘‘Clusters, Clumps, Gas, and Dust (CCDG) in Extreme Star-forming Galaxies’’ project (GO-15649; PI: Chandar). We use the ages and masses of the star cluster populations to trace the star formation process, because an increase in the rate of star formation results in an increase in the mass of the most massive clusters and in the amplitude of the cluster mass function (Chandar et al. 2017; Whitmore et al. 2020).

The rest of this paper is organized as follows. We summarize basic properties of our sample and the cluster catalogs in Section 2. In Section 3, we present the color–color diagrams, the mass–age diagrams, and the age distributions of the clusters. Section 4 focuses on estimating the star formation rate in different age intervals based on the observed cluster properties, and Section 5 presents the cluster-based star

formation histories of the BCDs, quantifies properties of bursts, and compares with known SFHs from more moderately star-forming dwarf galaxies. We summarize our main results in Section 6.

2. Galaxy Sample and Cluster Catalogs

This work is based on the new, HST-based cluster catalogs presented by Chandar et al. (2023) for ESO185, ESO338, and Haro11, also referred to as Paper I. In this section, we summarize basic properties of each galaxy and of the cluster catalogs; we refer the interested reader to Paper I for more details.

2.1. Blue Compact Dwarfs

In this work, we use observations of the BCD galaxies ESO185, ESO338, and Haro11 taken with the Hubble Space Telescope (HST), as part of the CCDG project (GO-15649, PI: Chandar). These galaxies are known to have formed many stellar clusters (e.g., Östlin et al. 2003; Adamo et al. 2010, 2011a, 2011b; Sirressi et al. 2022). Figure 1 shows color images of each galaxy. We adopt the same values for the distance, star formation rate (SFR), and SFR per area (Σ_{SFR}) for each galaxy as in Paper I and compiled in Table 1.

ESO185 has a bright, bar-like structure crossing the center, and tidal features that suggest it experienced a recent interaction or merging event. We adopt a distance of 76 Mpc, and estimate an $H\alpha$ -based star formation rate⁸ of $4.6 M_{\odot} \text{ yr}^{-1}$ and an SFR per unit area or $\Sigma_{\text{SFR}} = 0.38 M_{\odot} \text{ yr}^{-1} \text{ kpc}^{-2}$

⁸ In Paper I, we corrected the SFRs downward by a factor of 1.38, in order to convert them to a Chabrier IMF from the assumed Salpeter IMF.

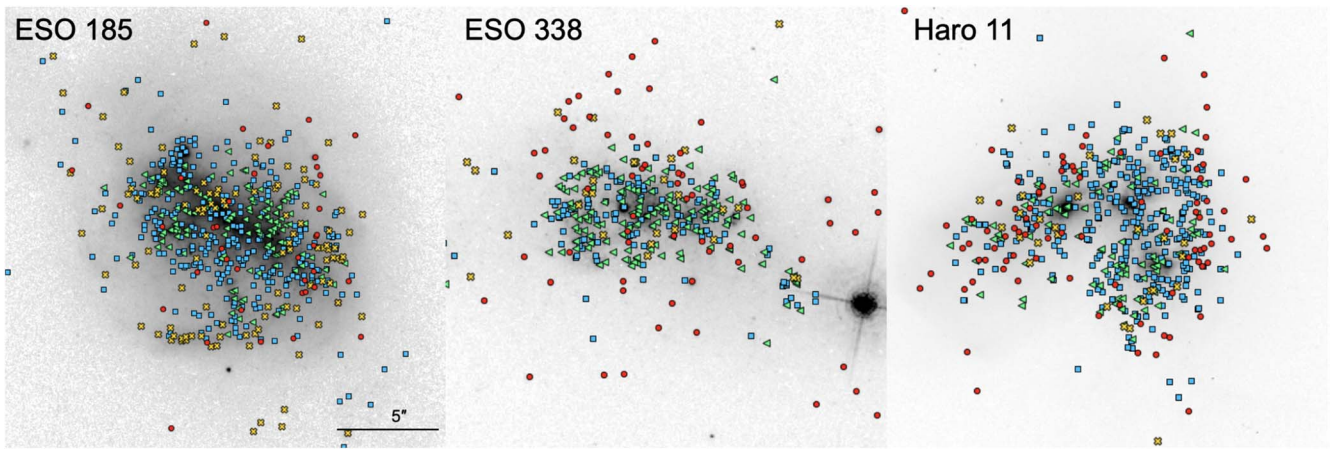


Figure 2. Locations of age-dated clusters in each target galaxy. Blue squares show very young clusters with estimated ages $\log(\tau/\text{yr}) \leq 7.0$, lime triangles represent $7.0 < \log(\tau/\text{yr}) \leq 8.0$, yellow crosses show $8.0 < \log(\tau/\text{yr}) \leq 8.6$, and red circles show the locations of clusters with $\log(\tau/\text{yr}) > 8.6$. Younger sources tend to be more clustered, and older clusters are preferentially found toward the outskirts of each system. The older clusters in the outskirts of ESO338 are particularly striking and easy to see in the images.

(Adamo et al. 2011a; Chandar et al. 2023). Very young, recently formed clusters are evident from the strong $\text{H}\alpha$ emission shown in red in Figure 1.

Recent star formation in ESO338 has been more evenly spread throughout the galaxy than in ESO185. This galaxy is located 38 Mpc away, and it has a previously estimated $\text{H}\alpha$ -based star formation rate of $2.3 M_{\odot} \text{yr}^{-1}$ and $\Sigma_{\text{SFR}} = 1.15 M_{\odot} \text{yr}^{-1} \text{kpc}^{-2}$ (Adamo et al. 2011b; Chandar et al. 2023). An earlier study by Östlin et al. (2003) found little-to-no obscuration by dust for even the youngest clusters formed in this galaxy.

Haro11 has three bright “knots” (labeled A, B, C), which are dominated by clusters of different ages (Sirressi et al. 2022). The region to the west of knot “B” has the strongest $\text{H}\alpha$ emission (shown in red in Figure 1) and has some dust and obscuration, although we do not identify any new clusters in this area from our near-infrared imaging. Knot A contains less $\text{H}\alpha$ emission and slightly older clusters, while Knot C has little $\text{H}\alpha$ emission and even older clusters. Haro11 is located at a distance of 82 Mpc, and it has an estimated $\text{H}\alpha$ -based star formation rate of $17.4 M_{\odot} \text{yr}^{-1}$ and $\Sigma_{\text{SFR}} = 1.70 M_{\odot} \text{yr}^{-1} \text{kpc}^{-2}$ (Adamo et al. 2011a; Chandar et al. 2023).

2.2. Source Detection and Photometry

HST images of ESO185, ESO338, and Haro11 are available in broad- and narrowband filters from the near-ultraviolet to the near-infrared. The observations used in this work are a mix of new and archival images. We use images in the following filters: *NUV* (F275W), *U* (F336W), *B* (ACS/F435W or WFC3/F438W), *V* (F555W), $\text{H}\alpha$ (F658N), and *I* (F814W). *P* β (F130N) and *H* (F160W) imaging taken with the WFPC3/IR camera as part of GO-15649 was not used in our age dating, because including these bands increased the uncertainties in the age-dating results (summarized below), likely due to the poorer resolution. Individual exposures are processed through the standard Pyraf/[0]STSDAS CALACS or CALWFC3 software, which performs initial data quality flagging, bias subtraction, gain correction, and bias stripe removal, corrects for CTE losses, and subtracts dark current. It then performs flat-fielding and photometric calibration on the images. The individual files are aligned and drizzled onto a common grid to create one image for each filter, with the *V*-band image used as the

reference. The images are all oriented with north up and east to the left, and they are shown in Figure 1.

At the distances of the three BCDs, stellar clusters appear as point-like sources. The DAOFIND detection algorithm was used to select point-like sources down to a 3σ detection limit. Aperture photometry in all broadband filters was performed in a two-pixel radius with background radii of 7 and 9 pixels. We convert the apparent magnitudes to the VEGAMAG system, but refer to them as the *NUV*, *U*, *B*, *V*, *I*, and $\text{H}\alpha$ filters for simplicity. Filter-dependent aperture corrections were determined from isolated sources and applied to obtain the total apparent magnitude for each cluster.

The main contaminants to the source lists are foreground stars and background galaxies. Most foreground stars are identified through GAIA astrometry. We performed a final visual inspection of all detected sources to remove any remaining contaminants. Some background galaxies are seen toward the outskirts of each system, and ESO185 and Haro11 each contain objects that appear to be nuclei or nuclear clusters (a single object at the dynamical center of ESO185, and three very bright point sources in Haro11). We do not include these sources in our catalogs. The final cluster catalogs contain 213/596 (ESO185), 300/399 (ESO338), and 180/536 (Haro11) candidate clusters brighter than $m_V = 24.5/27.0$ mag. The locations of the clusters in our final sample are shown in Figure 2.

2.3. Cluster Age and Mass Estimates

A detailed description of the age and mass estimates of the clusters was given in a companion work (Chandar et al. 2023), so we provide only a summary here. We estimated the age (τ) and extinction (A_V) for each cluster by performing a least- χ^2 fit comparing the observed cluster magnitudes (*NUV*, *U*, *B*, *V*, *I*, and $\text{H}\alpha$) with predictions from the $1/5 \times$ solar BC03 population model, where the measurement in each filter is weighted by the inverse of its photometric uncertainty. Adamo et al. (2010, 2011a) adopted a similar metallicity for these galaxies in their analysis of their cluster systems. The allowed cluster ages range from $\log(\tau/\text{yr}) = 6.0$ to 10.2, and the range of $E(B - V)$ runs from 0.0 mag up to a maximum value. For all clusters in ESO185 and ESO338, we adopt a maximum $E(B - V)$ value of 0.1 mag, because their colors closely follow the predicted evolutionary tracks, indicating they are hardly

affected by dust. We adopt the same maximum $E(B - V)$ for clusters in Haro11, except those in the dusty region around knot B, where we adopt a maximum $E(B - V) = 0.5$ mag, since some of these clusters have $H\alpha$ emission but redder colors.

Haro11 is the dustiest of the BCDs in our study, so it provides a good test for the results of our age dating. Figure 2 shows that clusters in knot B predominantly have ages younger than 10 Myr, those in knot A have ages just older than this, ≈ 10 –40 Myr, and those in knot C are older still, with ages ≈ 50 –400 Myr. This age progression can be clearly seen in Figure 1, where essentially no $H\alpha$ emission is seen in association with the clusters in knot C, weak $H\alpha$ emission is observed in knot A but not directly associated with most clusters, and strong $H\alpha$ emission is evident throughout knot B. Optical spectroscopy also supports these relative age estimates for the three knots (Sirressi et al. 2022).

We also ran our age-dating method with a maximum $E(B - V) = 1.0$ and 1.5 mag. We find that the age estimates for clusters with clear $H\alpha$ emission in ESO185 and Haro11 are almost always $\lesssim 6$ Myr, regardless of the maximum allowed $E(B - V)$ ⁹. This correct but nonetheless counterintuitive age-dating result occurs because strong $H\alpha$ emission tends to dominate over the fainter short-wavelength measurements in the fits. The main change in the age-dating results when the maximum $E(B - V)$ is set to 1.0 or 1.5 is that a number of clearly older clusters (based on their integrated colors, locations in less-crowded regions, and lack of dust or $H\alpha$ emission) are erroneously assigned young ages ≈ 7 –10 Myr and $E(B - V)$ values greater than 0.5 mag, instead of ages older than ≈ 100 Myr (see also Whitmore et al. 2020, 2023).

The mass of each cluster is estimated from the observed V -band luminosity, corrected for extinction. The (present-day) age-dependent mass-to-light ratios (M/L_V) are predicted by the models, assuming the distances compiled in Table 1. The BC03 models assume a fully sampled Chabrier (2003) stellar IMF with a range of masses between 0.1 and 100 M_\odot .

We made several detailed checks in Paper I and found that our method and assumptions result in good age estimates for the overall population, with no obvious systematic errors or biases. In Figure 2, we show the locations of clusters with different ages. Clusters tend to clump together when they are very young, and spread out over time. Older clusters are found preferentially toward the outskirts of the BCDs: ESO338, in particular, has a strong population of bright red, older clusters in the outskirts. While we may be missing faded, older clusters in the regions with bright backgrounds, we would not miss young clusters outside of these regions.

3. Results

3.1. Color–Color Diagrams

The color–color diagrams of cluster populations can reveal important information about the star formation histories of their host galaxies. We show the NUV – B versus V – I color–color diagrams of all detected clusters in ESO 185 (left panel), ESO 338 (middle panel), and Haro11 (right panel) as gray circles, and clusters brighter than m_V of 24.5 mag as black circles, in Figure 3. Cluster colors have been corrected for the foreground reddening values given in Table 1. The arrow in the right panel

shows the direction and amount that additional reddening of $E(B - V) = 0.4$ mag would move a cluster in this diagram, assuming a Milky Way–type extinction law (Fitzpatrick 1999).

Each panel also shows predictions from the Bruzual & Charlot (2003) stellar population models for $1/5 \times$ solar (solid line) and solar metallicity (dashed line). The models predict the color (and luminosity) evolution of clusters starting soon after their birth at 1 Myr (upper left), through the ages of globular clusters around ~ 12 Gyr in the lower right. The different metallicity models are reasonably similar at younger ages, but they diverge appreciably starting around a few $\times 100$ Myr, with bluer colors for a given age predicted at lower metallicity, the well-known age–metallicity degeneracy.

Intriguingly, there are notable differences in the colors of the cluster populations in the three BCDs studied here. A few key features are highlighted by the red circles in the top panels of Figure 3. ESO 338 has a rich population of clusters with colors between model ages of few $\times 100$ Myr and few Gyr, unlike either ESO 185 or Haro 11 (see the circled cluster population in the top middle panel of Figure 3). These are also seen in Figure 2 (middle panel) as the red circles found throughout—but preferentially on the outskirts of—the galaxy. An inspection of the images confirms that these are redder, older clusters rather than background galaxies. A number of clusters in ESO185 have colors that clump near the ~ 100 Myr model (circled in the top left panel of Figure 3), and the vast majority of bright clusters in Haro11 have colors that coincide with models younger than ≈ 30 Myr. As we will see below, these features observed in the color–color diagrams translate to the ages and masses of the cluster populations. There is a scatter of points, mostly faint clusters represented by gray dots that lie above the model predictions in a region of color–color space that cannot be explained by extinction due to dust. We examined these sources and almost all are quite faint with large uncertainties in the NUV photometry. These large uncertainties will downweight the NUV measurements in the age dating.

3.2. Mass–Age Diagram

In the bottom panels of Figure 3, we plot our age and mass results for the cluster populations of ESO185, ESO338, and Haro11, based on the SED fitting method described in the previous section. The dashed curve along the bottom of each distribution represents the approximate completeness limit of $M_V \approx -8$. This line essentially shows the fading of clusters over time, as luminosity-limited samples do not detect older clusters at lower mass, because they are significantly fainter than younger clusters at similar masses.

The mass–age diagrams have a number of small-scale features, with pileups at specific ages and small gaps at others. The broad distribution of cluster masses and ages, however, is not greatly affected by these small-scale features. The cluster populations in the three BCDs studied here show differences in their age–mass distributions, suggesting they have experienced distinct cluster and hence star formation histories over the past few Gyr. These differences reflect the key features we highlighted in their color–color diagrams. In Section 4, we determine the star formation rate in different age intervals for each galaxy. We adopt the following age intervals as our default: $\log(\tau/\text{yr}) = 6$ –7, $\log(\tau/\text{yr}) = 7$ –8, $\log(\tau/\text{yr}) = 8$ –8.6, and $\log(\tau/\text{yr}) = 8.6$ –9.5. If the cluster population looks fairly smooth across each age interval in the bottom panels of Figure 3 (for example, ESO338), we use the default age

⁹ The exception being a handful of very young but clearly reddened clusters in the dustiest region of Haro11, which requires an $E(B - V) = 0.5$, as described in Paper I.

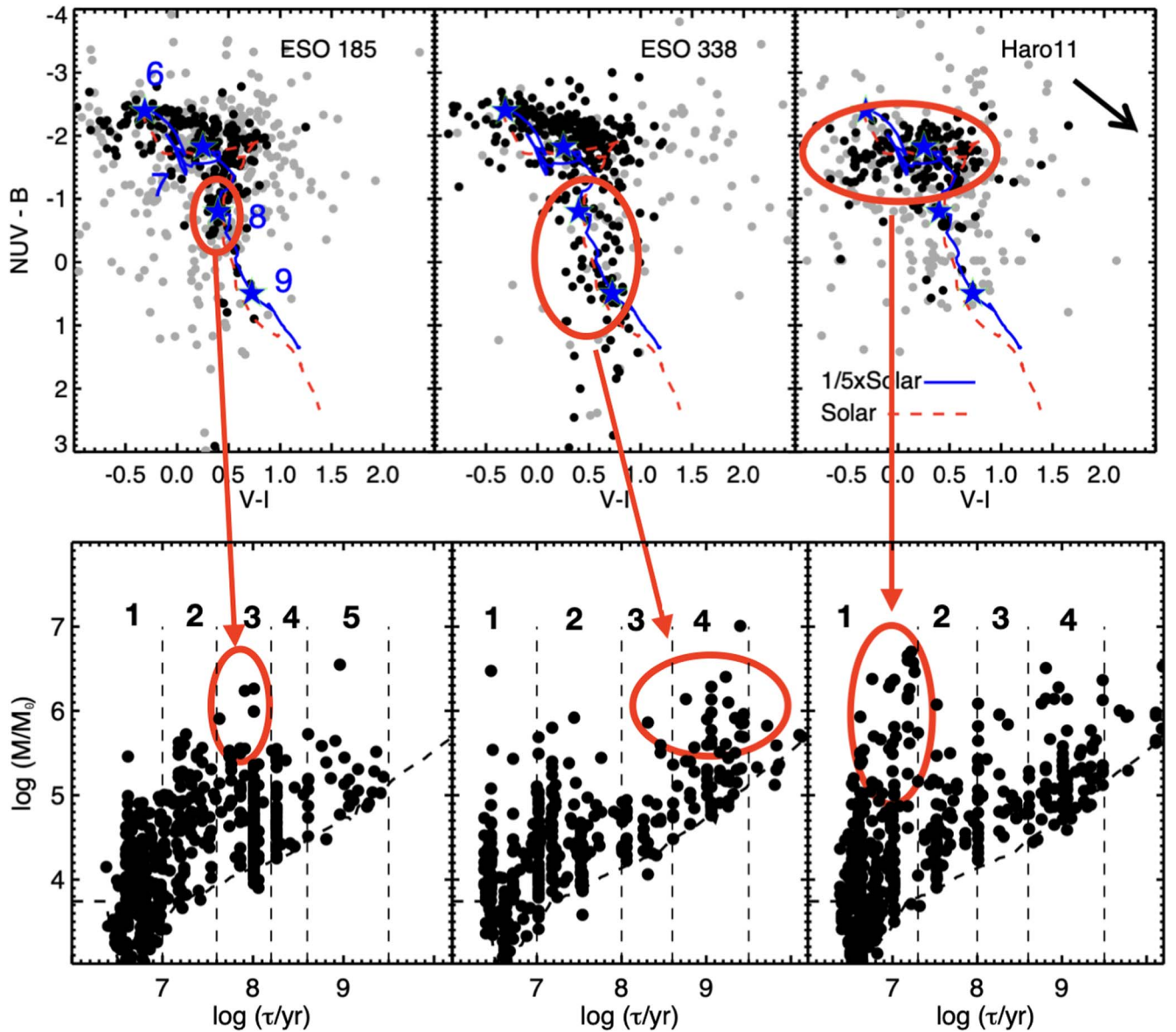


Figure 3. $NUV-B$ vs. $V-I$ color-color diagrams for the cluster populations in ESO185-IG13, ESO338-IG04, and Haro 11 are shown in the top panels, and the corresponding mass-age plots are shown in the bottom panels. Some key differences between the three blue compact dwarf galaxies are highlighted by the red circles and connected to the same cluster population in the age-mass diagrams. See text for more details.

intervals. If instead we see clear changes in the age-mass diagram (for example, the most massive clusters in Haro11 have ages between $\log(\tau/\text{yr}) \approx 6.7-7.3$), we customize the age interval so that these features do not get averaged out or diluted. This approach allows us to better quantify the timing, duration, and intensity of any bursts or enhancements in the star formation rate, which can occur at different times in different galaxies.

1. **ESO185** experienced strong cluster formation $\approx 15-40$ Myr ago (blue circle), and significantly less cluster formation earlier than $\approx \text{few} \times 100$ Myr ago. The clusters circled in red in the top left panel of Figure 3 correspond to an interval when cluster formation appears to have been enhanced relative to younger and older age intervals. Based on the age-mass diagram, we divide the cluster population into the following age intervals: $\log(\tau/\text{yr})$ of 6.0–7.0, 7.0–7.6, 7.6–8.2, 8.2–8.6, and

8.6–9.5. The star formation rate will be estimated separately for each of these intervals in Section 4.

2. **ESO338** has experienced much more continuous cluster formation than ESO185 over the past few Gyr, especially at ages older than $\gtrsim 100$ Myr. The highest masses reached by clusters in ESO338 are similar to those observed in spiral galaxies. We use the default age intervals for this population: $\log(\tau/\text{yr})$ of 6.0–7.0, 7.0–8.0, 8.0–8.6, and 8.6–9.5.
3. **Haro 11** experienced its strongest cluster formation only recently, with the most massive clusters forming approximately 15–20 Myr ago. In fact, the population includes clusters with some of the highest masses known in the nearby Universe, comparable to those found in NGC 1365 (Whitmore et al. 2023), the Antennae (Whitmore et al. 2010), and NGC 3256 (Mullia et al. 2016), all of which are systems with high rates of star

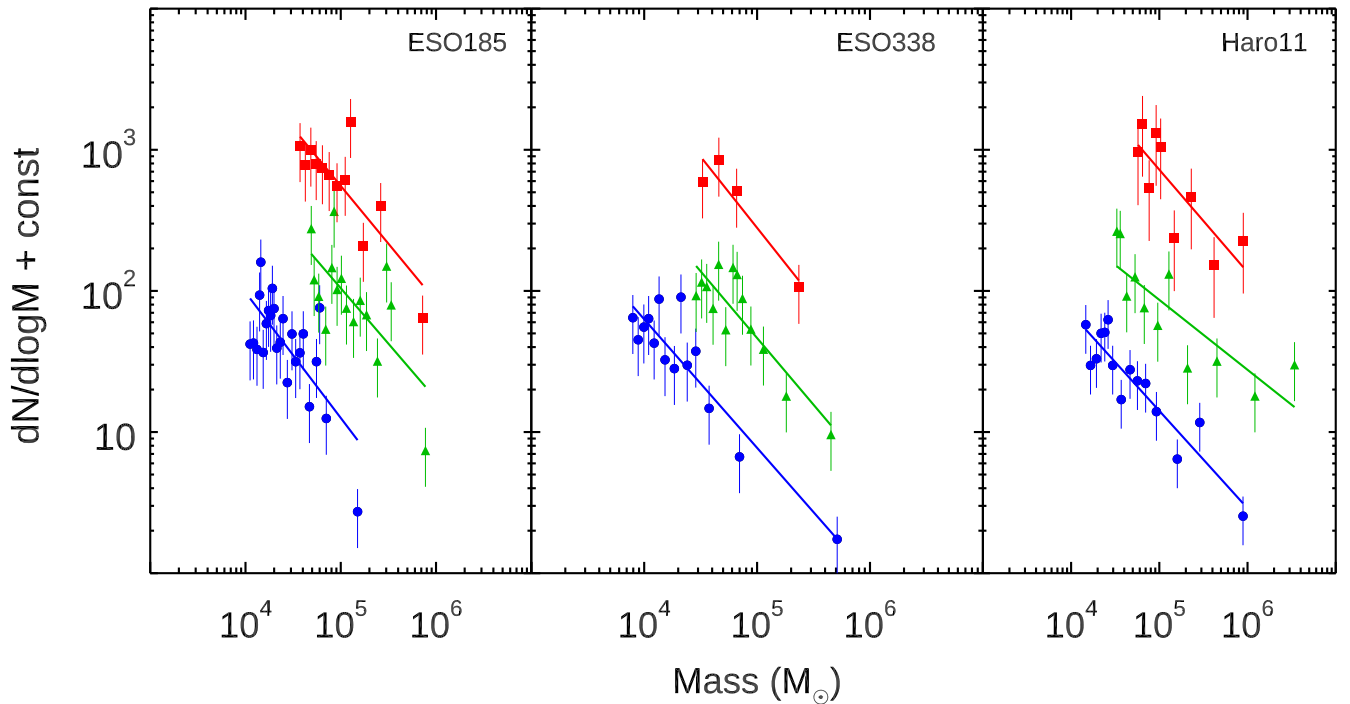


Figure 4. The shapes of the cluster mass functions in <10 Myr (blue), 10–100 Myr (green), and 100–400 Myr clusters (red) do not depend on age for our target galaxies, since we do not see older clusters (red) flatten toward lower masses, as expected if mass-dependent disruption dominates the shape of the cluster mass function. The best-fit power-law indices β for each distribution are as follows. ESO185: -1.89 ± 0.19 (1–10 Myr), -1.79 ± 0.23 (10–100 Myr), and -1.82 ± 0.18 (100–400 Myr). ESO338: -1.91 ± 0.11 (1–10 Myr), -1.95 ± 0.16 (10–100 Myr), and -2.01 ± 0.25 (100–400 Myr). Haro11: -1.69 ± 0.08 (1–10 Myr), -1.49 ± 0.11 (10–100 Myr), and -1.73 ± 0.21 (100–400 Myr).

formation. We study the Haro11 cluster population in the following age intervals: $\log(\tau/\text{yr})$ of 6.0–7.3, 7.3–8.0, 8.0–8.6, and 8.6–9.5.

3.3. Mass and Age Distributions

The cluster mass and age distributions and their relationships to one another provide important insight into the formation and evolution of the clusters (e.g., Bastian et al. 2005; Chandar et al. 2010; Fall et al. 2010; Fall & Chandar 2012).

In Figure 4, we present the mass functions for star clusters in three intervals of age, 1–10 Myr (blue), 10–100 Myr (green), and 100–400 Myr (red), for each of our galaxies. Each mass function is well described by a simple power law, $dN/d \log M \propto M^{\beta+1}$, and all but one have a best-fit value within $\beta = -1.9 \pm 0.2$ (compiled in Table 2). The one exception is for clusters formed between 10 and 100 Myr ago in Haro11, which have a somewhat flatter distribution with $\beta = -1.50 \pm 0.11$. This could be, at least in part, because there are several very massive clusters (approaching $\approx 10^7 M_\odot$), which flatten the upper end of the distribution. Another possibility is that the difficulty in identifying fainter, lower-mass clusters in galaxies beyond ≈ 50 Mpc due to crowding can result in a power-law index that is flatter by ~ 0.3 (Lahén et al. 2022). Overall, however, the shapes of the cluster mass functions are quite similar at different ages, and they are approximately independent of age.

Lahén et al. (2022) also find that, during an intense star-forming event, the most massive clusters may have masses that are overestimated by a factor up to ≈ 3 in galaxies beyond 50 Mpc. Because clusters disperse over time, we do not expect this bias to persist for more than a few tens of Myr. We assess the impact this bias may have on 10–100 Myr clusters in

Table 2
Power-law Index (β) for Cluster Mass Function Fits

Galaxy Name	β 1–10 Myr	β 10–100 Myr	β 100–400 Myr
ESO 185	-1.89 ± 0.19	-1.79 ± 0.23	-1.82 ± 0.18
ESO 338	-1.91 ± 0.11	-1.95 ± 0.16	-2.01 ± 0.25
Haro11	-1.69 ± 0.08	-1.49 ± 0.11	-1.73 ± 0.21

Note. The power-law index is determined from a least-squares fit to $\log(dN/d \log M) = (\beta + 1)\log M + \text{const}$.

Haro11 by performing a simple experiment where we assume that each of the 10 most massive clusters are actually made up of three equal-mass clusters. The experimental catalog gives a mass function that has a power-law index that is steeper by ≈ 0.2 .

The observed age distribution reflects the combined formation and disruption histories of the clusters. If clusters form at a constant rate with little-to-no disruption, their age distribution, $\chi(\tau) \propto dN/d\tau \propto \tau^\gamma$, will be flat, with $\gamma \approx 0$. If mass-dependent disruption is important in shaping cluster demographics, lower-mass clusters will disrupt earlier than their higher-mass counterparts, leading to a steeper power-law index for lower-mass clusters. For constant formation and mass-independent disruption, $\gamma < 0$, with no dependence of γ on cluster mass. Alternatively, $\gamma < 0$ could also arise from an increasing rate of cluster formation from the past to the present.

Figure 5 shows cluster age distributions in the indicated mass intervals for each BCD. We have used bin sizes in $\log \tau$ that are a compromise between bridging small-scale features in the M – τ diagram and small-number statistics, while also restricting the plotted ranges to stay above the luminosity limit of each cluster

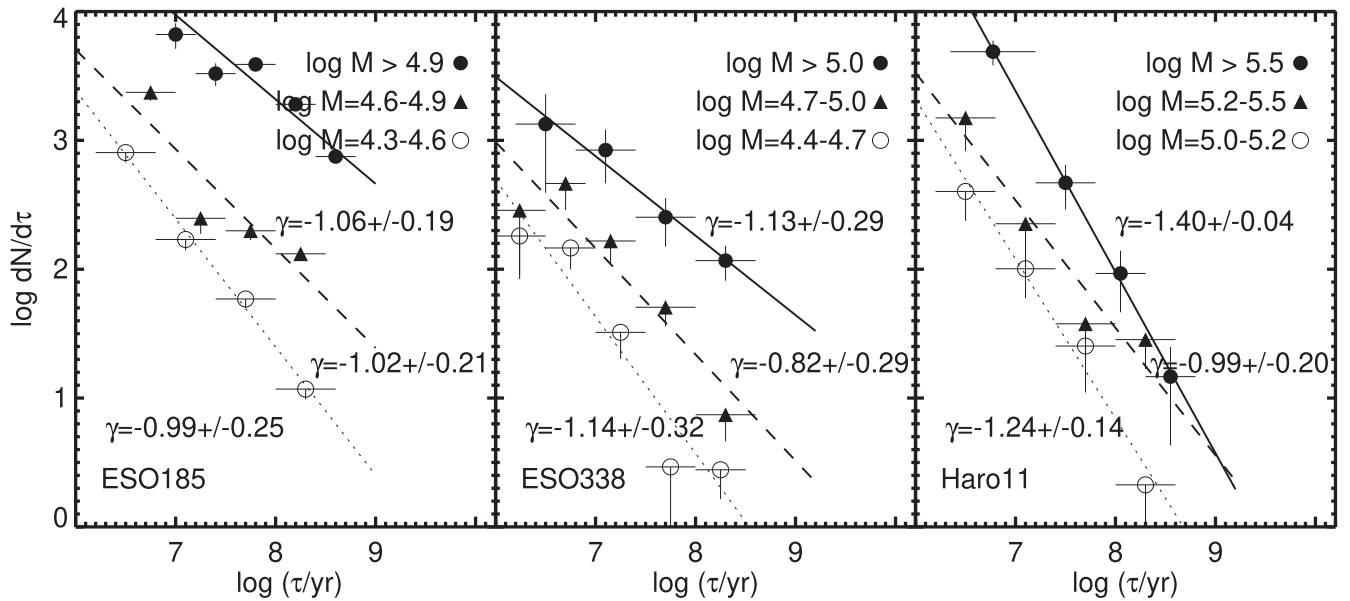


Figure 5. The cluster age distributions do not depend on mass, because their shapes are approximately similar in different mass ranges (indicated). If mass-dependent disruption affected the observed cluster population, lower-mass clusters should have a steeper age distribution than their higher-mass counterparts. The lines show power laws, $dN/d\tau \propto \tau^\gamma$, with the best-fitting exponents written by each distribution.

Table 3
Power-law Index (γ) for Cluster Age Distribution Fits

Galaxy Name	Mass Range 1 $\log(M/M_\odot)$	γ_1	Mass Range 2 $\log(M/M_\odot)$	γ_2	Mass Range 3 $\log(M/M_\odot)$	γ_3
ESO 185	>4.9	-1.06 ± 0.19	4.6 – 4.9	-1.02 ± 0.21	4.3 – 4.6	-0.99 ± 0.25
ESO 338	>5.0	-1.13 ± 0.29	4.7 – 5.0	-0.82 ± 0.29	4.4 – 4.7	-1.14 ± 0.32
Haro11	>5.5	-1.40 ± 0.04	5.2 – 5.5	-0.99 ± 0.20	5.0 – 5.2	-1.24 ± 0.14

Note. The power-law index is determined from a least-squares fit to $\log(dN/d \log \tau) = (\gamma) \log \tau + \text{const.}$

sample. All plotted distributions decline continuously starting at very young ages. This is not surprising, given the distribution of cluster colors discussed in Section 2. We perform a linear fit to each distribution for the power-law index γ as $\log dN/d\tau = \gamma \times \log(\tau/\text{yr})$. We find that all three BCDs have steep age distributions, with typical values of $\gamma = -1.0 \pm 0.2$ (compiled in Table 3). Haro11 has the steepest cluster age distribution, dominated by the youngest data points. This likely reflects the intense, ongoing star and cluster formation in this galaxy. Although the uncertainties are fairly large for some of the distributions, we do not find any obvious differences for the power-law index γ in the different mass intervals within any of the galaxies. We conclude that shapes of the cluster age distributions are approximately independent of their masses.

We find that, overall, the cluster age distributions in ESO185, ESO338, and Haro11 have declining shapes similar to those in irregular, spiral, and merging galaxies (Fall & Chandar 2012), modulo increases in age intervals where there are clear enhancements in the cluster populations. This suggests that the cluster disruption histories are similar to those found for cluster populations in other galaxies, and for these BCDs the differences mostly reflect differences in their formation histories.

4. Estimates of Star Formation Rate

The masses and ages of clusters can be used to estimate the star formation rate of their host galaxy under the assumptions that star and cluster formation are proportional to one another

and that the mass and age distributions are independent of one another. Chandar et al. (2015, 2017) showed that, when the observed cluster mass function for eight very different galaxies is divided by the star formation rate, the resulting distributions lie nearly on top of one another, at least for clusters with ages up to ≈ 400 Myr, and possibly up to a few Gyr. By essentially reversing this approach, we have developed a new method to estimate the rate of star formation from the observed cluster mass function in specified age intervals (Chandar et al. 2021, 2023).

In this method, the rate of star formation (within a specific age interval) is determined from the vertical normalization of the cluster mass function, with a higher normalization attributed to a higher rate of star formation. As a consequence, the masses of the most massive clusters generally correlate with the normalization of each mass function, with higher normalizations and hence rates of star formation resulting in more massive clusters, because each distribution follows a power law with $\beta \approx -2$ (see Section 3.3). One strength of this approach is that it uses the majority of the observed cluster population to determine the SFH.

The cluster populations in the BCDs studied in this work have a proportionality between stars and clusters, similar to that found in galaxies studied by Chandar et al. (2015, 2017). Our method to estimate star formation rate in a given age interval is demonstrated in Figure 6. In the left panel, we show the observed mass function for clusters in a specified age interval (in this case, 1–10 Myr) for our calibration galaxies: the SMC

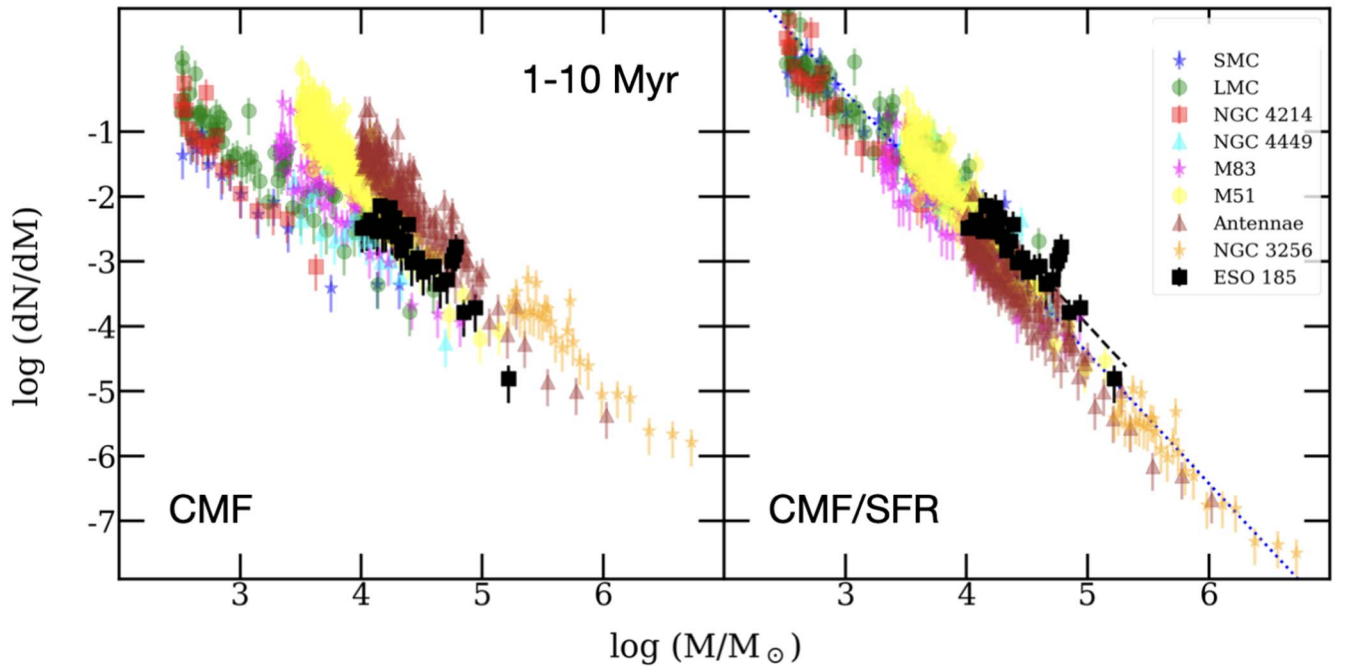


Figure 6. This figure demonstrates the CMF/SFR method used to estimate the star formation rate from the cluster mass functions in different age intervals. In the left panels, we show the observed mass functions of clusters in eight calibration galaxies, in the 1–10 Myr age intervals, and that for ESO185-IG13 in black squares. The right panels show that, when the CMFs of the calibration galaxies are divided by their SFRs, the resulting CMF/SFR distributions lie nearly on top of one another. The data points for ESO185-IG13 are the same in both panels. In the right panel, the dashed line shows the best fit to 1–10 Myr clusters in ESO185-IG13, which lies above the dotted line showing the best fit to the eight calibration galaxies or an SFR of $1 M_{\odot} \text{ yr}^{-1}$. The dotted calibration line has a power-law index $\beta = -2.01 \pm 0.02$ and a y-intercept of 643.4 ± 24.4 .

and LMC (irregulars), NGC 4214 and NGC 4449 (dwarf starbursts), M83 and M51 (spirals), and Antennae and NGC 3256 (mergers). The $H\alpha$ -based SFRs in these galaxies (compiled in Table 1 in Chandar et al. 2017) span a factor of nearly 1000, which is reflected in their very different vertical scales. The right panel shows that, when divided by SFR, the cluster mass functions for these very different galaxies collapse to form essentially a single relation.

The calibration to estimate SFR from an observed CMF can be determined for any age interval as follows. The cluster mass function for each of the eight calibration galaxies is constructed and divided by the SFR. A single power-law fit to all data points is performed to establish the best-fit values and statistical errors for the power index β and the y-intercept or vertical normalization. This normalization value corresponds to an SFR of $1 M_{\odot} \text{ yr}^{-1}$ and is different for different age intervals.

The vertical offset of an observed cluster mass function relative to the $1 M_{\odot}$ calibration line determines the SFR and its associated uncertainties, which depend on errors in the observed CMF and in the calibration itself. The statistical uncertainty for the best-fit normalization of the CMF/SFR for all eight calibration galaxies is $\approx 3.5\%$, with variations at the 1% level for age intervals used in this work. We assess the validity of these statistical uncertainties from a simple “bootstrap” experiment, where we calculate the best-fit y-intercept or normalization using seven (instead of eight) of the calibration galaxies for all combinations. The standard deviation of y for this set is comparable to (within 50%, sometimes smaller and sometimes larger than) the statistical uncertainties for y from fits using all eight calibration galaxies. For example, for the age interval $\log(\tau/\text{yr}) = 6.0\text{--}7.0$, the power-law fit to CMF/SFR for all eight calibration galaxies is $y = 643 \pm 23$, whereas the standard deviation from the bootstrap experiment is 33. This

test suggests that the statistical uncertainty in the fit to the normalization value y is reasonable.

In Figure 6, the black circles show that the mass function of 1–10 Myr clusters in ESO 185 falls closest to that observed for M83 (pink stars) and M51 (yellow triangles), which have estimated SFRs of $1.6 M_{\odot} \text{ yr}^{-1}$ and $2.9 M_{\odot} \text{ yr}^{-1}$, respectively (see Chandar et al. 2017 for details). To estimate the rate of star formation in ESO 185 from 1 to 10 Myr, a power law with the same index as found from the fit to the combined CMF/SFR distribution from the calibration galaxies in the same age interval is fitted to the observed 1–10 Myr cluster mass function. This procedure results in an average SFR of $2.7 \pm 0.9 M_{\odot} \text{ yr}^{-1}$ for ESO185 over the 1–10 Myr age interval, quite similar to the SFRs of M83 ($1.6 M_{\odot} \text{ yr}^{-1}$) and M51 ($2.9 M_{\odot} \text{ yr}^{-1}$). The uncertainties are calculated by propagating (adding in quadrature) the statistical uncertainties in the normalization y from the calibration and from the fit to the observed cluster mass function.

We perform a consistency check of our method by comparing the cluster-based SFR estimates for the 1–10 Myr age interval with those determined from the total $H\alpha$ + infrared luminosity for each BCD studied here. Both methods use tracers of similar-age stellar populations. We find good agreement between the two: our cluster-based method (global $H\alpha$ +IR luminosity) returns estimates of the star formation rate of $2.7 \pm 0.9 M_{\odot} \text{ yr}^{-1}$ ($4.6 M_{\odot} \text{ yr}^{-1}$) for ESO185, $1.7 \pm 0.7 M_{\odot} \text{ yr}^{-1}$ ($2.3 M_{\odot} \text{ yr}^{-1}$) for ESO338, and $17 \pm 5 M_{\odot} \text{ yr}^{-1}$ ($17.4 M_{\odot} \text{ yr}^{-1}$) for Haro11. In all three cases, our cluster-based SFR estimates are within a factor of 1.7 of those determined from the total $H\alpha$ + IR luminosity of the host galaxy, giving additional confidence in our cluster-based method. We apply this method to estimate the SFR in each age interval listed in Section 3.2 for ESO185, ESO338, and Haro 11.

Table 4
Star Formation Rate Estimates

Galaxy Name	Age Bin 1 Norm. SFR	Age Bin 2 Norm. SFR	Age Bin 3 Norm. SFR	Age Bin 4 Norm. SFR	Age Bin 5 Norm. SFR
ESO 185	$\log(\tau/\text{yr}) = 6 - 7$	$\log(\tau/\text{yr}) = 7 - 7.6$	$\log(\tau/\text{yr}) = 7.6 - 8.2$	$\log(\tau/\text{yr}) = 8.2 - 8.6$	$\log(\tau/\text{yr}) = 8.6 - 9.5$
ESO 185	$1051 \pm 168 \ 2.7 \pm 0.9$	$680 \pm 41 \ 11.5 \pm 4.5$	$1492 \pm 86 \ 2.7 \pm 1.0$	$1177 \pm 52 \ 3.0 \pm 1.7$	$1520 \pm 49 \ 0.7 \pm 0.4$
ESO 338	$\log(\tau/\text{yr}) = 6 - 7$	$\log(\tau/\text{yr}) = 7 - 8$	$\log(\tau/\text{yr}) = 8 - 8.6$	$\log(\tau/\text{yr}) = 8.6 - 9.5$...
ESO 338	$840 \pm 160 \ 1.7 \pm 0.7$	$2169 \pm 383 \ 3.2 \pm 1.3$	$1359 \pm 44 \ 0.8 \pm 0.5$	$1520 \pm 49 \ 1.6 \pm 0.6$...
Haro11	$\log(\tau/\text{yr}) = 6.0 - 7.3$	$\log(\tau/\text{yr}) = 7.3 - 8.0$	$\log(\tau/\text{yr}) = 8.0 - 8.6$	$\log(\tau/\text{yr}) = 8.6 - 9.5$...
Haro11	$686 \pm 16 \ 27.6 \pm 17.0$	$1200 \pm 37 \ 1.6 \pm 0.9$	$1539 \pm 47 \ 2.4 \pm 1.9$	$1520 \pm 49 \ 2.4 \pm 1.0$...

Notes. The age bins used for each galaxy are reported on the first line, and the best-fit normalization or y-intercept to the observed CMF and the resulting SFR are reported on the second line. See text for more details.

The best-fit normalization and uncertainty, as well as the resulting star formation rate estimate for each age interval, are compiled in Table 4.

5. Star Formation Histories of Blue Compact Dwarf Galaxies

We are interested in answering basic questions about the star formation histories (SFHs) of BCDs, which may inform our understanding of the star formation histories experienced by distant, young galaxies. We are interested to know: (1) are all BCDs currently experiencing a burst of star formation? (2) What are the frequencies, durations, and strengths of bursts of star formation in BCDs and how do burst properties compare with those found in dwarf starbursts and irregulars that are forming stars at more modest rates? (3) How long and “quiescent” are periods between bursts in BCDs?

In Figure 7, we present the first star formation histories for BCD galaxies using the cluster-based method described in the previous section. ESO338, shown in blue, has experienced a fairly constant SFH. This is not surprising, given that the cluster colors are quite continuous, as seen in the upper middle panel of Figure 3, starting from the very young blue end of the predicted colors in the upper left and extending down to model ages of several Gyr toward the lower right. The estimated SFR of $\approx 1.6\text{--}3.2 M_{\odot} \text{yr}^{-1}$ over the past few Gyr is similar to that found in spiral galaxies like M83 and M51, but occurring within a radius smaller by a factor of ≈ 10 and an area (and hence Σ_{SFR}) smaller by a factor of ≈ 100 .

Figure 7 indicates that ESO185 has also experienced a fairly constant star formation history over the past few Gyr, but with one enhanced star formation episode that started ≈ 40 Myr ago and persisted for ≈ 30 Myr. This duration is quite similar to that of bursts identified in simulations of post-starburst galaxies (which are on the order of ~ 25 Myr; see, e.g., French et al. (2018) and references therein). The star formation rate increased by a factor of ≈ 4 during this enhanced star-forming period, from $\approx 2.7 M_{\odot} \text{yr}^{-1}$ before and after the burst to $\approx 11.5 M_{\odot} \text{yr}^{-1}$ during it. Approximately 1–3 Gyr ago, ESO185 had the lowest rate of star formation out of the three BCDs, with very few clusters observed around these ages.

Haro11 has the highest current rate of star formation out of the three BCDs studied here, with an average of $27 \pm 7 M_{\odot} \text{yr}^{-1}$ over the past ≈ 20 Myr. We note that this is higher than we estimated for the 1–10 Myr interval in Section 4, because the most massive clusters—and hence the highest rate of star formation—occurred closer to ≈ 20 Myr ago. This rate is higher than found in some actively merging systems like the Antennae. Haro11 is also the only one out of

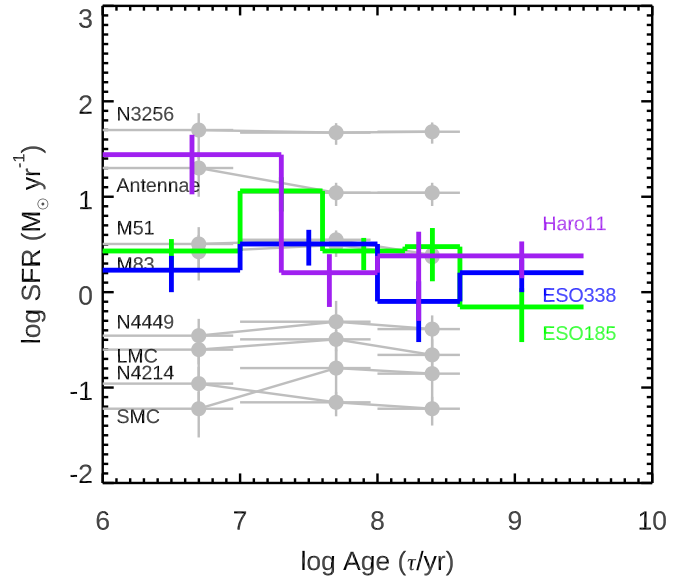


Figure 7. The cluster-based star formation history of ESO185 (green), ESO338 (blue), and Haro11 (purple), determined as described in Section 5 are shown. The histories determined for the eight labeled galaxies from integrated light measurements (not clusters) and presented in Chandar et al. (2017) are shown for comparison in gray.

these three galaxies that is currently experiencing a sharp increase or burst of star formation. This burst started ≈ 20 Myr ago and continues to the present day. At that time, the SFR increased from $\sim 2 M_{\odot} \text{yr}^{-1}$ to $\sim 27 M_{\odot} \text{yr}^{-1}$, or by a factor of ≈ 10 .

Overall, our cluster-based SFHs for the three BCDs studied in this work do not follow the canonical picture, wherein a BCD experiences long periods of quiescence occasionally punctuated by an intense burst of star formation. Our results also indicate that not all BCDs are experiencing a current “burst” of star formation, and that some may not have experienced a burst at all over the past ≈ 0.5 Gyr and possibly the past few Gyr. Although our sample is small, ESO185, ESO338, and Haro11 have each experienced unique star formation histories. ESO185 experienced a factor-of-four enhancement in star formation, while Haro 11 experienced a burst that represents an increase in the star formation rate that is approximately a factor of 10. While the intensities differ, both of these star-forming episodes appear to have been short-lived, lasting only a few tens of millions of years—although the burst in Haro11 appears to be ongoing, so we do not yet know its total duration. The star-forming knots in Haro11 have physical sizes of ≈ 1 kpc (Sirressi et al. 2022). Assuming a “signal

speed” of $\sim 30 \text{ km s}^{-1}$ (Whitmore et al. 1999), these knots have a crossing time on the order of \approx a few tens of Myr, consistent with the estimated duration of the burst in Haro11.

Our results do not support previous suggestions that ESO185, ESO338, and Haro11 are all currently experiencing a peak in their rate of star formation that started ≈ 3 Myr ago (Östlin et al. 2003; Adamo et al. 2011a). Our conclusion also seems reasonable based on statistical arguments, given that the past 10 Myr constitutes just 1/1000 of the ages of galaxies and the probability of catching a number of galaxies all experiencing a burst of star formation in the past few million years is extremely low.

McQuinn et al. (2010a, 2010b) found that dwarf irregular and starburst galaxies located within 10 Mpc do not appear to experience short-lived (≈ 5 –10 Myr) “bursts” of star formation, as had long been believed, but rather they have experienced fairly constant star formation (within a factor of a few) over hundreds of Myr. Overall, Cignoni et al. (2019) find fairly constant SFRs over the past 100 Myr for 23 dwarf star-forming galaxies studied as part of the LEGUS survey, with enhancements only at the factor of 2–3 level. This conclusion was based on a very different approach from that used here, and it relied instead on analyzing the color–magnitude diagrams of individual stars. Our results indicate that, while BCDs have higher overall rates of star formation, many have experienced star formation histories that do not differ dramatically from their dwarf cousins that have lower rates of star-forming activity.

6. Conclusions

Blue compact dwarfs (BCDs) are small galaxies with low metallicity and little dust that are undergoing intense star formation. The canonical picture for these systems is one where BCDs experienced long periods of quiescence punctuated by short-lived, violent bursts of star formation. They are particularly interesting because they share many properties with young galaxies at high redshift, so their star formation histories provide a critical window into the evolution of dwarf galaxies. The cluster populations of BCDs can provide unique insight into their star formation histories.

In this work, we have used the ages and masses of the stellar clusters in ESO185, ESO338, and Haro11, three BCD galaxies, to determine their star formation histories over the past ≈ 3 Gyr. Each galaxy has a unique distribution of cluster colors that reflects its unique star and cluster formation history. We estimated the rate of star formation in different age intervals from a calibration between the well-studied cluster masses and star formation rates (SFR) in eight nearby star-forming galaxies. The SFRs estimated from our cluster-based method in the 1–10 Myr age interval are within a factor of 1.7 of those determined from the total $H\alpha$ luminosity of each galaxy. From estimates in several different intervals, we constructed star formation histories (SFHs) for each galaxy.

The star formation histories determined for these three BCDs provide important insight into this class of extreme galaxy. One conclusion is that the traditional picture of long gaps punctuated by short, intense bursts, including a burst at the present day, is not an accurate picture. We find that not all BCDs are bursting or experiencing their peak rate of star formation right now, and some BCDs (like ESO338) may not have experienced a burst or even a factor-of-four enhancement at all, at least over the past few Gyr. The fairly steady star

formation histories found for these three BCDs appears similar to that experienced by dwarf starburst and dwarf irregular galaxies, two classes of galaxy with star formation rates that are 10–10,000 times lower than ESO185, ESO338, and Haro11.

Haro11 is the only galaxy in this study that is currently experiencing a peak in its rate of star formation (estimated to be $27 \pm 7 M_{\odot} \text{ yr}^{-1}$), which represents a factor of ≈ 10 increase over its past rate. ESO185 experienced a much more modest increase of a factor ≈ 4 in its SFR, starting ≈ 40 Myr ago and ending ≈ 30 Myr later. These systems provide tentative evidence that increased periods of star formation may persist for timescales of ≈ 20 –30 Myr, consistent with the expected signal-crossing time of star-forming knots observed in BCDs, but this should be checked using larger samples.

We conclude that cluster populations are a promising approach for understanding the evolution of galaxies with unusual star formation histories.

Acknowledgments

We thank the anonymous referee for carefully reading and helping us improve our manuscript. R.C. acknowledges support from HST-GO-15649.

Software: Photutils (Bradley et al. 2020), Matplotlib (Hunter 2007), NumPy (Oliphant 2006; Van Der Walt et al. 2011), Astropy (Astropy Collaboration et al. 2022), SciPy (Virtanen et al. 2020), SAOImage DS9 (Smithsonian Astrophysical Observatory 2000).

ORCID iDs

Rupali Chandar  <https://orcid.org/0000-0003-0085-4623>

Miranda Caputo  <https://orcid.org/0000-0002-2957-3924>

Angus Mok  <https://orcid.org/0000-0001-7413-7534>

Sean Linden  <https://orcid.org/0000-0002-1000-6081>

Bradley C. Whitmore  <https://orcid.org/0000-0002-3784-7032>

Paul Goudfrooij  <https://orcid.org/0000-0002-5728-1427>

David O. Cook  <https://orcid.org/0000-0002-6877-7655>

Daniela Calzetti  <https://orcid.org/0000-0002-5189-8004>

Debra M. Elmegreen  <https://orcid.org/0000-0002-1392-3520>

Janice C. Lee  <https://orcid.org/0000-0002-2278-9407>

Leonardo Úbeda  <https://orcid.org/0000-0001-7130-2880>

Richard White  <https://orcid.org/0000-0002-9194-2807>

References

- Adamo, A., Östlin, G., & Zackrisson, E. 2011a, *MNRAS*, 417, 1904
- Adamo, A., Östlin, G., Zackrisson, E., & Hayes, M. 2011b, *MNRAS*, 414, 1793
- Adamo, A., Östlin, G., Zackrisson, E., et al. 2010, *MNRAS*, 407, 870
- The Astropy Collaboration, Price-Whelan, A. M., Lim, P. L., et al. 2022, *ApJ*, 935, 167
- Bastian, N., Gieles, M., Lamers, H. J. G. L. M., Scheepmaker, R. A., & de Grijs, R. 2005, *A&A*, 431, 905
- Bekki, K., Owers, M. S., & Couch, W. J. 2010, *ApJL*, 718, L27
- Bradley, L., Sipőcz, B., Robitaille, T., et al. 2020, *astropy/photutils*: 1.0.0, v1.0.0, Zenodo, doi:10.5281/zenodo.4044744
- Bruzual, G., & Charlot, S. 2003, *MNRAS*, 344, 1000
- Cairós, L. M., Caon, N., Zurita, C., et al. 2010, *A&A*, 520, A90
- Chabrier, G. 2003, *PASP*, 115, 763
- Chandar, R., Caputo, M., Mok, A., et al. 2023, *ApJ*, 949, 116
- Chandar, R., Fall, S. M., Whitmore, B. C., & Mulia, A. J. 2017, *ApJ*, 849, 128
- Chandar, R., Fall, S. M., & Whitmore, B. C. 2010, *ApJ*, 711, 1263
- Chandar, R., Fall, S. M., & Whitmore, B. C. 2015, *ApJ*, 810, 1

- Chandar, R., Mok, A., French, K. D., Smercina, A., & Smith, J.-D. T. 2021, *ApJ*, **920**, 105
- Chen, Z., Stark, D. P., Endsley, R., et al. 2023, *MNRAS*, **518**, 5607
- Cignoni, M., Sacchi, E., Tosi, M., et al. 2019, *ApJ*, **887**, 112
- Contreras Ramos, R., Annibali, F., Fiorentino, G., et al. 2011, *ApJ*, **739**, 74
- Fall, S. M., & Chandar, R. 2012, *ApJ*, **752**, 96
- Fall, S. M., Krumholz, M. R., & Matzner, C. D. 2010, *ApJL*, **710**, L142
- Fanelli, M. N., O'Connell, R. W., & Thuan, T. X. 1988, *ApJ*, **334**, 665
- Ferguson, H. C., & Babul, A. 1998, *MNRAS*, **296**, 585
- Fitzpatrick, E. L. 1999, *PASP*, **111**, 63
- French, K. D., Yang, Y., Zabludoff, A. I., & Tremonti, C. A. 2018, *ApJ*, **862**, 2
- Hainline, K. N., Johnson, B. D., Robertson, B., et al. 2024, *ApJ*, **964**, 71
- Harris, J., Calzetti, D., Gallagher, J. S., I., Smith, D. A., & Conelice, C. J. 2004, *ApJ*, **603**, 503
- Hoopes, C. G., Heckman, T. M., Salim, S., et al. 2007, *ApJS*, **173**, 441
- Hunter, J. D. 2007, *CSE*, **9**, 90
- Janowiecki, S., & Salzer, J. J. 2014, *ApJ*, **793**, 109
- Kunth, D., Maurogordato, S., & Vigroux, L. 1988, *A&A*, **204**, 10
- Lahén, N., Naab, T., & Kauffmann, G. 2022, *MNRAS*, **514**, 4560
- Lelli, F., Verheijen, M., & Fraternali, F. 2014, *MNRAS*, **445**, 1694
- Mas-Hesse, J. M., & Kunth, D. 1999, *A&A*, **349**, 765
- McQuinn, K. B. W., Skillman, E. D., Cannon, J. M., et al. 2010a, *ApJ*, **724**, 49
- McQuinn, K. B. W., Skillman, E. D., Cannon, J. M., et al. 2010b, *ApJ*, **721**, 297
- Mulía, A. J., Chandar, R., & Whitmore, B. C. 2016, *ApJ*, **826**, 32
- Oliphant, T. E. 2006, *A Guide to NumPy*, Vol. 1 (USA: Trelgol Publishing)
- Olsen, C. A., Gawiser, E., Iyer, K., et al. 2021, *AAS Meeting*, **53**, 331.08
- Östlin, G., Zackrisson, E., Bergvall, N., & Rönback, J. 2003, *A&A*, **408**, 887
- Papaderos, P., Guseva, N. G., Izotov, Y. I., & Fricke, K. J. 2008, *A&A*, **491**, 113
- Papaderos, P., Loose, H. H., Fricke, K. J., & Thuan, T. X. 1996, *A&A*, **314**, 59
- Sargent, W. L. W. 1970, *ApJ*, **159**, 765
- Schaerer, D., Contini, T., & Kunth, D. 1999, *A&A*, **341**, 399
- Silich, S., Tenorio-Tagle, G., Muñoz-Tuñón, C., & Cairos, L. M. 2002, *AJ*, **123**, 2438
- Sirressi, M., Adamo, A., Hayes, M., et al. 2022, *MNRAS*, **510**, 4819
- Smithsonian Astrophysical Observatory 2000, SAOImage DS9: A utility for displaying astronomical images in the X11 window environment, [ascl:0003.002](https://doi.org/10.2602/0003.002)
- Stinson, G. S., Dalcanton, J. J., Quinn, T., Kaufmann, T., & Wadsley, J. 2007, *ApJ*, **667**, 170
- Thornley, M. D., Förster Schreiber, N. M., Lutz, D., et al. 2000, *ApJ*, **539**, 641
- Thuan, T. X., & Izotov, Y. I. 2005, *ApJS*, **161**, 240
- Tosi, M., Greggio, L., & Focardi, P. 1989, *Ap&SS*, **156**, 295
- Tremonti, C. A., Calzetti, D., Leitherer, C., & Heckman, T. M. 2001, *ApJ*, **555**, 322
- van der Walt, S., Colbert, S. C., & Varoquaux, G. 2011, *CSE*, **13**, 22
- van Zee, L., Skillman, E. D., & Salzer, J. J. 1998, *AJ*, **116**, 1186
- Virtanen, P., Gommers, R., Oliphant, T. E., et al. 2020, *NatMe*, **17**, 261
- Whitmore, B. C., Chandar, R., Lee, J., et al. 2020, *ApJ*, **889**, 154
- Whitmore, B. C., Chandar, R., Rodríguez, M. J., et al. 2023, *ApJL*, **944**, L14
- Whitmore, B. C., Chandar, R., Schweizer, F., et al. 2010, *AJ*, **140**, 75
- Whitmore, B. C., Zhang, Q., Leitherer, C., et al. 1999, *AJ*, **118**, 1551
- Zhao, Y., Gu, Q., & Gao, Y. 2011, *AJ*, **141**, 68